Asynchronous control of vortex-induced acoustic cavity resonance using imbedded piezo-electric actuators ⊘

M. M. Zhang; L. Cheng; Y. Zhou

Check for updates

View
Online

Export
Citation

Articles You May Be Interested In

Closed-loop control of flow-induced sound in a flow duct with downstream resonant cavities

J. Acoust. Soc. Am. (March 2013)

Experimental investigation of the diffraction of sound by a curved surface of finite impedance

J Acoust Soc Am (August 2005)

Air entrapment in piezo-driven inkjet printheads

J. Acoust. Soc. Am. (September 2006)

Asynchronous control of vortex-induced acoustic cavity resonance using imbedded piezo-electric actuators

M. M. Zhang,[a)] L. Cheng,[b)] and Y. Zhou

Department of Mechanical Engineering, The Hong Kong Polytechnic University, Hung Home, Kowloon, Hong Kong, SAR of China

This paper presents an experimental investigation of the control of a vortex-induced acoustic cavity resonance from flow over a bluff body using embedded piezo-ceramic actuators in order to alter the resonant flow-acoustic interactions. The action of the actuators was asynchronous. Experiments were mainly conducted at the flow velocity of acoustic resonance, where the vortex shedding frequency from the upstream bluff body approached the frequency of the first acoustic mode of two downstream cavities. The fluctuating acoustic pressure was measured using a microphone. The perturbed flow field around the bluff body was monitored using two single hot wire anemometers and one *X*-wire. It was found that the induced transverse vibrations were effective to reduce the acoustic resonance. The cavity sound pressure level at resonance was reduced by 8.2 dB in presence of actuation. The physics behind the control mechanism is discussed.
© 2009 Acoustical Society of America. [DOI: 10.1121/1.3143784]

I. INTRODUCTION

Flow-induced acoustic resonance occurs as a result of strong interactions between unsteady separated flows and the acoustic modes of a cavity, when the dominant frequency of the flow separation approaches that of one acoustic mode of the cavity.[1–6] This phenomenon is commonly found in many engineering applications, and may be classified into self-induced and vortex-induced resonances. The former is excited by vortices shed from the orifice leading edge over the cavity, and often occurs in landing-gears, weapon bays in aircraft, and open cavities in moving vehicles. The latter is caused by vortex shedding from a bluff body in crossflows and is frequently seen in tube or plate bundles of heat exchangers and boilers,[7] cascades of compressor blades,[8] and guide/turning vanes in ducts and radial diffusers.[9] Flow-induced acoustic resonance may induce an acoustic pressure amplitude sufficiently high to cause very serious noise or vibration problems.[10]

Control of self-induced resonance has been extensively explored using passive and active control techniques.[11] Typical passive methods include modifications of the geometries of the acoustic source regions,[12,13] use of fences or screens within the cavities,[14,15] and use of small leading edge spoilers to control the source.[9] In contrast, active control techniques involve energy input via actuators to manipulate the shear flow, effectively reducing the flow-acoustic interaction, using either independent external disturbance, i.e., open-loop control, or feedback-signal-controlled system, i.e., closed-loop control. Active control techniques can be synchronous or asynchronous, depending on whether the actuation frequency is equal to the system fundamental frequency.[16] To mention a few typical examples, Sarno and Franke[17] successfully suppressed shear layer oscillations in a cavity through 45° steady or pulsating mass flow injection at the cavity leading edge, resulting in a reduction of 10 dB in the cavity sound pressure level (SPL) at the frequency of the acoustic resonance. Using a closed-loop method, Huang and Weaver[18] and Ziada *et al.*[19] used the fluctuating acoustic pressure inside the cavity as feedback signals, which was then amplified and phase-shifted by a controller to drive control loudspeakers at the entrance of the tunnel and at the upstream corner of the cavity, respectively. In this way, the shear layer oscillation across the cavity was attenuated. Cattafesta *et al.*[16,20,21] and Kook *et al.*[22] used an oscillating piezo-electric flap and electrodynamically driven leading edge spoilers, respectively, which were hinged near the cavity leading edge, to disturb the shear layer separation. The action of the flap was controlled by a closed-loop controller with the feedback signals from the fluctuating acoustic pressure within the cavity. As a result, attenuation in cavity pressure was obtained at the frequency of acoustic resonance.

Control of vortex-induced acoustic resonance has been scarcely reported in the literature, apart from a few papers reporting numerical simulations of the phenomenon. This phenomenon may be important in cascade structures, such as turbines, helicopters, and fans, in which a blade interacts with the wake of an upstream blade; the other is the occurrence of acoustic resonance, as evidenced by Mohany and Ziada[10] who measured the acoustic resonant interaction between vortices shed from an upstream cylinder and the first acoustic mode of the tunnel where the cylinder was located and obtained a SPL of 155 dB in a wind tunnel and the work of Roozen *et al.*[23] in which strong vortex-induced noise was measured near the bass-reflex port of a loudspeaker. Their work was mainly focused on investigations of acoustic-structure coupling rather than control.

[a)]Present address: Department of Mechanical Engineering, Johns Hopkins University, 3400 N. Charles Street, Baltimore, MD 21218.
[b)]Author to whom correspondence should be addressed. Electronic mail: mmlcheng@polyu.edu.hk

Vortex-induced acoustic resonance induced by vortex shedding from bluff bodies may possibly be controlled by effectively impairing the source, i.e., vortex shedding. Many investigations of passive and active control of vortex shedding from bluff bodies have been reported in the literature. Passive control methods typically include changing the cross section of structures and adding fixed mechanical vortex disturbers such as longitudinal grooves or riblets to alter vortex shedding.[24–26] As examples of active open-loop control, Hsiao and Shyu[27] used acoustic waves emitted from a slot on the surface of a cylinder to actively disturb the fluid field and demonstrated that a local disturbance near the shear layer instability frequency and around the flow separation point caused an increase in lift and a reduction in drag and the vortex strength (Re=420–34 000). Williams *et al.*[28] introduced symmetric and anti-symmetric forcing of water flow (Re=470) at a frequency of about twice the vortex shedding frequency (f_s) through two rows of holes located at $\pm45°$, respectively, away from the forward stagnation line of the cylinder. They observed a change in shedding frequency and flow structure. Most existing closed-loop vortex shedding control methods rely on feedback signals provided by hot wires in the turbulent wake. Warui and Fujisawa[29] reduced the vortex strength at Re=6700 using electromagnetic actuators installed at both ends of a circular cylinder to create a lateral oscillation. Tokumaru and Dimotakis[30] and Filler *et al.*[31] created cylinder rotary oscillations to produce regulated injection of circulation into the wake. Both led to an attenuation in vortex strength and drag. Ffowcs Williams and Zhao[32] used a loudspeaker mounted on a wind tunnel wall to impair vortex shedding from a cylinder at Re=400. Using the same technique, Roussopoulos[33] observed an increase by 20% in the onset Reynolds number for vortex shedding. Huang[34] used sound within a cylinder to generate a pulsating flow through a thin slit near the separation point on the cylinder surface, and suppress vortex shedding from both sides of the cylinder in the Re range between 4×10^3 and 1.3×10^4.

Cheng *et al.*[35] developed a novel perturbation technique to control both vortex shedding and structural vibration. The essence of the technique is to generate a controllable transverse motion of a structural surface using embedded piezoceramic actuators to alter fluid-structure interactions. The effectiveness of this technique has been demonstrated for the case of active control of vortex shedding and associated structural vibrations for different cases of fluid-structure interactions, including resonant flow-structure coupling on a flexible-supported rigid cylinder,[36,37] resonant flow-structure coupling on a fix-supported flexible cylinder,[38] and nonresonant coupling on a fix-supported flexible cylinder.[39] This technique has recently been successfully applied to the control of noise caused by blade-vortex interaction[40] (BVI) and the control of airfoil aerodynamics.[41] Piezo-ceramic actuators are lighter and smaller than other actuation devices such as loudspeakers and electromagnetic actuators. Owing to its special design, the actuator presently used requires a relatively low energy input to generate appreciably large dis-

placements. Typically, without any loading, it can vibrate at a maximum displacement of about 2 mm and a frequency up to 2 kHz.

This paper presents results from an experimental study to extend the aforementioned technique to the control of the vortex-induced acoustic resonance by means of reducing vortex strength by a bluff body. Asynchronous control was carried out in this study to establish the feasibility of the technique. The test configuration comprises an upstream bluff body acting as the vortex generator, and two downstream acoustic cavities, within which acoustic resonance phenomenon occurs. Experiments were focused on the occurrence of acoustic resonance when the vortex shedding frequency coincided with the frequency of the first acoustic resonance of the cavity. Uncontrolled flow-acoustic interactions were first investigated. A simple asynchronous control system was developed. Control performance was assessed in terms of the cavity SPL at resonance. To understand the control mechanism, the perturbed flow field and the resonant flow-acoustic interaction were analyzed in detail.

II. EXPERIMENTAL PROCEDURES

Experiments were carried out in a closed circuit wind tunnel, as shown in Fig. 1(a). This facility, designed for aeroacoustic experiments, was previously used for flow-silencer testing.[42] It has a 1.82-m-long square test section of 0.1×0.1 m^2. A parabolic contraction at the inlet improved the uniformity of the flow velocity profile and reduced boundary layer thickness. A flat-walled diffuser, with a half angle of $14°$, was used downstream of the working section to increase pressure recovery. The maximum flow velocity was 50 m/s with a turbulence intensity of less than 0.1% in the upstream section. The background noise of the tunnel was low since the motor and fan noise was mostly absorbed by acoustic lining. This has been experimentally verified.

A rigid thick rectangular plate, with a height of $h=11$ mm, a width of $w=47$ mm, and a length of 98 mm, was used as bluff body. The plate was rigidly fixed on both side walls of the test section and located about 0.37 m downstream of the exit plane of the tunnel contraction, as shown in Figs. 1(a) and 1(b). The plate angle of attack was zero. Note that w/h was about 4.3, falling into the range between 3.2 and 7.6, where only one vortex separated from the leading edge of the plate may develop along the plate at any instant. This is a typical pattern of flow around a rectangular plate.[43] To improve the two-dimensionality of vortex shedding from the plate, the cross section of the plate leading edge was made semi-circular[44] [Fig. 1(b)]. Two identical cavities with square cross sections were located downstream of the plate, symmetrical with respects to x-z plan, on the top and bottom walls of the tunnel, respectively, and at the same streamwise location. The two cavities act as side-branch acoustic resonators. The origin of the coordinate system, shown in Fig. 1(a), was defined at the center of the model trailing edge, with x, y, and z corresponding to the streamwise, transverse, and spanwise directions, respectively. The depth (L) and width (B) of each cavity were 440 and 70 mm, respectively. The first acoustic resonance frequency of the

FIG. 1. Experimental setup: (a) Wind-tunnel and sensing configuration; (b) test model in detail; (c) asynchronous control system and measurement system.

cavity (f_a') was approximately $f_a'=c/4L\approx193.2$ Hz,[45] where c is the speed of sound. The corresponding critical flow velocity U_{cr} ($=f_s h/\mathrm{St}$) at resonance, when shedding frequency $f_s=f_a'$, was estimated to be about 8.5 m/s, using a Strouhal number St of 0.25, as suggested by Welsh *et al.*[44] for similar w/h ratios. The distance between the trailing edge of the plate and the downstream wall of the cavities was about

9.8h. This distance ensured an effective resonant fluid-acoustic interaction in the near wake of the plate, as demonstrated later.

Two curved piezo-ceramic actuators [thin layer composite unimorph driver and sensor (THUNDER)],[46] with a length of 63 mm and a width of 14 mm, were embedded in a slot of 80 mm long, 30 mm wide, and 7 mm deep on the top side of bluff body and 1.5 mm from the model trailing edge [Fig. 1(b)]. The two actuators were installed at $x=-1.41$ to 0.14h and $x=-2.77$ to $-1.50h$ [Fig. 1(b)], respectively. The characteristics of the actuators have been thoroughly discussed previously.[46] Typically, without any loading, the present actuator (THUNDER-8R) can vibrate with a peak displacement of about 2 mm and a frequency up to 2 kHz. The actuators were installed in a cantilever manner to create the maximum perturbation displacement in the transverse y-direction, and thus better control performance for the same excitation condition. The actuators and the walls of the slot around the actuators were lubricated to minimize contact friction. A thin plastic plate with a thickness of 1.2 mm, mounted flush with the upper surface of the plate, was connected with the cantilevered end of the actuators using double-sided glue and was placed at $x=-2.82$ to $-0.091h$ [see Fig. 1(b)]. Driven by the actuators, the plate oscillated to create a uniform transverse vibration of the plate surface, as confirmed by the measurement of velocity at several points over the place by a laser vibrometer. The motion of the plate may have created a small step on the test model surface. But the gap between the plate and the model was small such that leakage effects were deemed negligibly small. Furthermore, the plate had a maximum displacement of less than 0.9 mm, and was rather stiff. Therefore, spanwise variation in transverse displacement (80 mm) due to the actuators could be neglected. The actuators were simultaneously activated by a sinusoidal signal with controllable frequency. The input voltage was generated by a simple asynchronous control system, including a signal generator (Model DS345) and a dual-channel piezo-driver amplifier (Trek PZD 700), as indicated in Fig. 1(c).

A 12.7 mm diameter condenser microphone (B&K 4189), mounted flush with the center of the top wall of the upper cavity [Fig. 1(a)], was used to measure the fluctuating acoustic pressure inside the cavity. To analyze the control effect on the flow field, one or two tungsten single hotwires of 5 μm in diameter, with wire aligned with z direction, were deployed to measure the fluctuating flow velocity and streamwise mean velocity. Figure 1(a) shows a typical arrangement of one single wire case, placed at $x/h=2$ and $y/h=1.5$. Furthermore, the fluctuating flow velocities along x- and y-directions in the wake of the test model were measured using a 5 μm tungsten X-wire. The measured flow velocities were corrected using the method of Durgun and Kafali,[47] in view of the present blockage ratio ($\approx11\%$). In addition, the perturbation displacement (Y_p) was measured using a Polytec Series 3000 dual beam laser vibrometer [Fig. 1(a)]. After amplification, all measurement signals were recorded using a personal computer through a 12-bit AD board at a sampling frequency of 6 kHz per channel. The duration of each record was about 20 s.
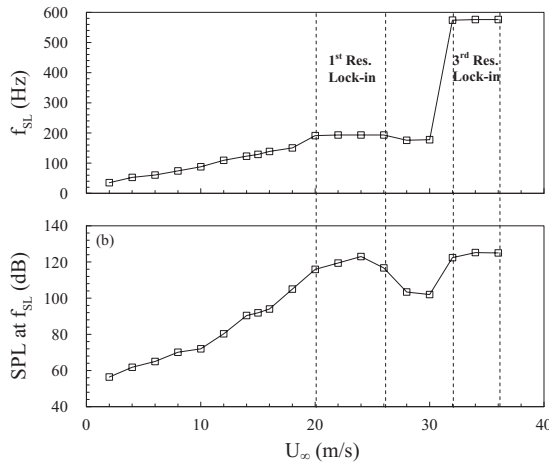
FIG. 2. Dependence of the frequency of the shear layer (f_{SL}) separated from the two cavities (a) and SPL at f_{SL} (b) on the free-stream flow velocity (U_∞) in the absence of the test model.

III. UNCONTROLLED FLOW-ACOUSTIC INTERACTION

Uncontrolled flow-acoustic interactions were first examined to provide a baseline for comparison. As previously mentioned, in the present setting, one would expect the sound inside the cavity to be induced by both self-induced resonance and vortex-induced resonance. It is therefore important to ensure that the two cases have very different critical flow velocities so that they can be separated. In view of this, a test was first conducted before the installation of the bluff body to investigate the variation of the frequency of the shear layer (f_{SL}) separated from the two cavities and SPL at f_{SL} with the free-stream flow velocity U_∞, as shown in Fig. 2. It can be seen from Fig. 2(a) that f_{SL} generally increased with U_∞. Two plateaus appear within the velocity ranges of $U_\infty=20-26$ m/s and $U_\infty=32-36$ m/s [Fig. 2(a)], where f_{SL} is locked-in to the first and third acoustic mode frequencies of the cavity, i.e., $f_a'(=193.4$ Hz) and $f_a'''(=576.2$ Hz), respectively. The first range matches the theoretical prediction of the critical flow velocity corresponding to the first mode resonance [$U_{cr}=21.3$ m/s, calculated from $U_{cr}=f_a'B\pi/(4St)$,[48] with St=0.5 (Ref. [45])]. The SPL at f_{SL} is rather high, up to 126 dB, in the two lock-in ranges, suggesting the occurrence of strong resonance. Note that the second acoustic resonance mode was not excited, which is consistent with the analyses on acoustic resonance in a cavity with one closed end by Morse.[49]

Similar experiments were repeated after the test model was installed. Figure 3 illustrates the dependence of the frequency of the vortices shed from the test model (f_s), SPL at f_s and the magnitude of the power spectrum of the fluctuating flow velocity E at f_s on the free-stream flow velocity (U_∞). The hotwire was located at $x/h=1$ and $y/h=0.75$, where the flow velocity fluctuation was observed to be very strong. Although the lock-in phenomenon under the first-mode acoustic resonance still exists, the flow velocity range corresponding to $f_a'(=193.4$ Hz), i.e., 8.3 m/s $<U_\infty<9.2$ m/s, obviously becomes narrower, consistent with observation of Welsh et al..[44] Recall that the calculated $f_a'(=193.2$ Hz) is very close to the measured value and the calculated $U_{cr}(=8.5$ m/s) lies in the lock-in range from 8.3 to 9.2 m/s,
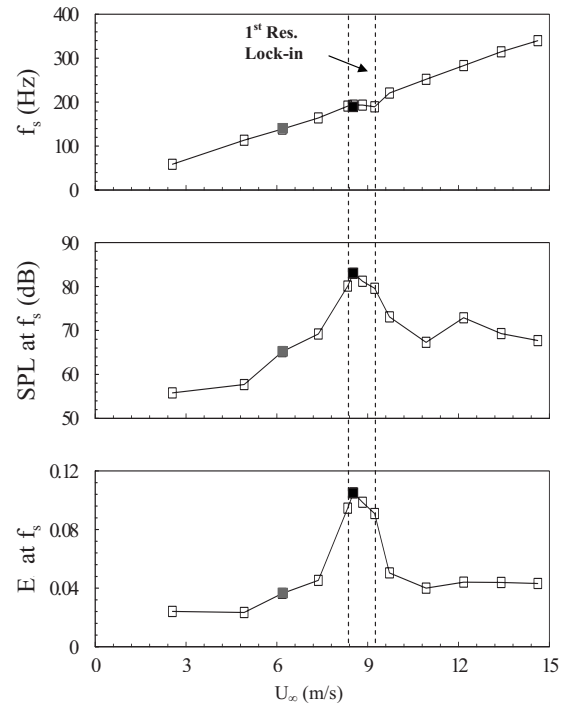
FIG. 3. Dependence of the frequency of the vortices shed from the test model (f_s), SPL at f_s and the magnitude of the power spectrum of the fluctuating flow velocity E at f_s on the free-stream flow velocity (U_∞) in the presence of the test model. The hot wire was located at $x/h=1$ and $y/h=0.75$.

in reasonable agreement with the measurement. Furthermore, for 8.3 m/s $<U_\infty<9.2$ m/s, the averaged SPL at f_s is about 81 dB when the test model is installed (Fig. 3). Clearly, the oscillations caused by self-induced resonance and the vortex-induced resonance have very different critical flow velocities so that their effects can be easily separated. The strongest acoustic resonance was observed at $U_\infty=8.53$ m/s, corresponding to a Reynolds number Re ($\equiv U_\infty h/\nu$, where ν is the kinematic viscosity) of 6200, where both the SPL at f_s and the E at f_s reach their maximum value of 83 dB and 0.11, respectively. This working condition was chosen as the control target in the following control tests.

IV. CONTROL PARAMETERS AND PERFORMANCES

Two important parameters, i.e., the perturbation frequency f_p and perturbation voltage V_p of the controller need to be determined. To this end, a series of tests was conducted to document the effect of these two parameters on the SPL at f_a', i.e., the strength of the vortex-induced acoustic resonance. Figure 4(a) shows the variation of the SPL at f_a' and the root mean square (rms) value of perturbation displacement Y_{prms} with f_p. A maximum permissible voltage, with a rms value $V_{prms}=141$ V, was applied to the actuators as f_p varied within $0-90$ Hz. In this low frequency range, the noise generated by the actuator itself, if any, was undetectable by the microphone. Compared with the unperturbed case ($f_p=0$ Hz and $V_{prms}=0$ V), the SPL at f_a' was reduced when the actuation was employed. The maximum attenuation occurred at $f_p=30$ Hz, resulting in a reduction of 8.2 dB in the SPL. At a fixed $f_p(=30$ Hz), Fig. 4(b) shows the variation of the
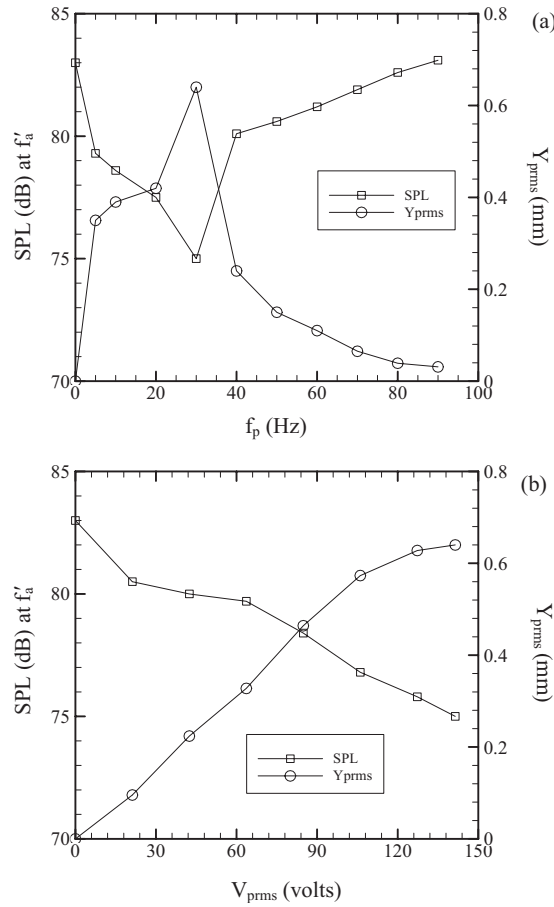
FIG. 4. Effect of control parameters on the SPL at f'_a and the rms value of the perturbation displacement Y_{prms}: (a) different perturbation frequency f_p at $V_{prms} = 141$ V; (b) different V_{prms} at $f_p = 30$ Hz. Re=6200.
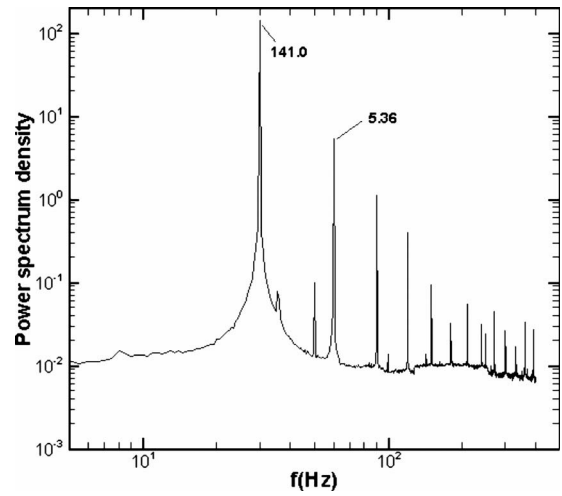

FIG. 5. Power spectrum of perturbation when the perturbation frequency f_p was 30 Hz and rms value of perturbation voltage V_{prms} is 141 V.

SPL at f'_a and Y_{prms} with V_{prms}. It can be seen that the SPL at f'_a monotonously decreased as V_{prms} was increased from 0 to 141 V. Obviously, a greater actuation voltage is desirable. Further iterations between f_p and V_{prms} failed to improve the control performance significantly, implying that the combination of $f_p = 30$ Hz with $V_{prms} = 141$ V were the optimum parameters for the asynchronous controller. In fact, the natural frequency of the actuator presently used was designed to be around 30 Hz, at which the rms value of the perturbation displacement Y_{prms} was largest, up to about 0.64 mm [Fig. 4(a)]. In addition, Y_{prms} increased monotonously with V_{prms} [Fig. 4(b)], though not linearly.[50] The large Y_{prms} may partially account for the better control authority at $f_p = 30$ Hz and $V_{prms} = 141$ V over other combinations of f_p and V_{prms}. Unless otherwise stated, this optimum set of parameters was used in the experiments hereinafter. The power spectral density of the surface oscillating velocity was measured using the laser vibrometer, as shown in Fig. 5. It has been observed that the actuation-produced surface oscillation is predominately controlled by its first harmonic component at 30 Hz. Other harmonics are all below 4% of the dominant frequency. Therefore, the surface motion could be approximately considered to be simple harmonic.

The control performance of the above tuned asynchronous controller was further evaluated in terms of the power spectrum of SPL at f'_a. Figure 6 shows the results, with and without control, at Re=6200. Four evident peaks in the SPL-spectrum appear in the absence of control, corresponding to the natural frequency of shear layer separation, i.e., f'^*_{SL}, the frequencies of the first, third, and fifth cavity acoustic modes, i.e., f'^*_a (=vortex shedding frequency f'^*_s), f'''^*_a, and $f^{(5)*}_a$, respectively. The asterisk used in this paper denotes the normalization of frequency f by h and U_∞, i.e., $f^* = fh/U_\infty$. As mentioned before, only odd modes of the cavity appear. Figure 6 shows that, under control, the SPL at $f'^*_a = f'^*_s$ decreases from 83 to 74.8 dB, although a small peak at $f^*_p = 0.039$ emerges, apparently due to the excitation. In addition, reductions in the SPL at f'''^*_a and $f^{(5)*}_a$ are also noticeable. Generally, the control was deemed to be effective.

V. DISCUSSIONS

To understand the underlying physics, the perturbation effect on the flow field in the wake of the test model was examined. Figure 7 displays the power spectrum, E, of fluctuating flow velocity with and without perturbation. The
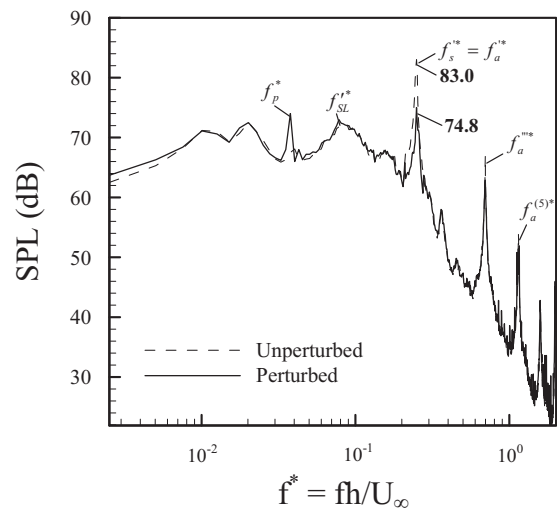

FIG. 6. Spectrum of SPL with and without perturbation. The perturbation frequency and the rms value of perturbation voltage were 30 Hz and 141 V, respectively. Re=6200.
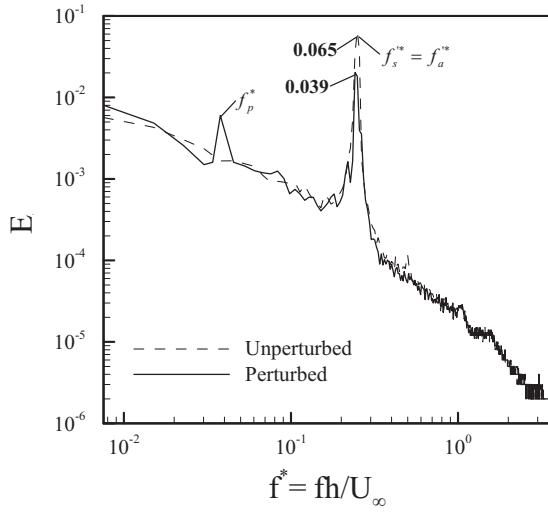
Zhang *et al.*: Control of acoustic cavity resonance

FIG. 7. Power spectrum, E, of the fluctuating flow velocity with and without perturbation (Re=6200). The hotwire was located at $x/h=1.5$ and $y/h=1$.

FIG. 8. Cross-flow distribution of mean streamwise flow velocity and Reynolds stresses at $x/h=2$: (a) $\bar{U}*$, (b) $\overline{u^2}*$, (c) $\overline{v^2}*$, (d) $\overline{uv}*$. Re=6200.

spectra were normalized in this paper so that $\int_0^\infty E(f)df=1$. The hotwire was placed at $x/h=1.5$ and $y/h=1$. Without perturbation, a pronounced peak, due to vortex shedding from the test model, occurred at $f_s'^*=f_a'^*=0.25$ in E. The peak magnitude at $f_s'^*$ was 0.065. Upon the deployment of control, the peak magnitude at $f_s'^*$ was reduced to 0.039 or around 5 dB, i.e., 60% of its unperturbed counterpart, suggesting an effective impairment in the energy of the vortices. In order to make sure the control does not affect the flow only locally, Fig. 8 compares the cross-flow distributions of the mean velocity $\bar{U}*$ and the Reynolds stresses $\overline{u^2}*$, $\overline{v^2}*$, and $\overline{uv}*$ measured by an X-wire at $x/h=2$ with and without perturbation. Compared with the unperturbed case, the minimum $\bar{U}*$ and maximum $\overline{u^2}*$, $\overline{v^2}*$ and $\overline{uv}*$ exhibit a considerable decrease by 9.3%, 21.6%, 36.7%, and 38.9%, respectively. The similar control effect is still discernible at $x/h=5$, as shown in Fig. 9. Clearly, the vortex strength in the wake of the model is impaired. The increased mean velocity deficit in $\bar{U}*$ is related to the decreased entrainment of high speed fluid from the free-stream, which is induced by the weakened vortex strength.[29] Furthermore, the reduced maximum $\overline{u^2}*$, $\overline{v^2}*$ and $\overline{uv}*$ may be ascribed to the impaired vortex strength.

It is pertinent to mention that the ability of the present technique in suppressing vortex formation from bluff bodies and reducing vorticity has been demonstrated using extensive particle image velocimetry (PIV) measurement in the past.[35–39] Although the present test model differs from the ones used in the previous studies, the basic phenomenon should remain the same. According to Howe's vortex sound theory,[3] the reduction in vortex circulation strength is responsible for the noise source reduction.

Insight may be better gained into the impairment in the vortex strength by examining how the flow around the test model evolves and responds to the control. Figure 10 shows the control effect on the fluctuating flow velocity spectrum E at different streamwise locations with constant $y/h=0.75$. Before perturbation, a very small peak in E (0.0014 in mag-
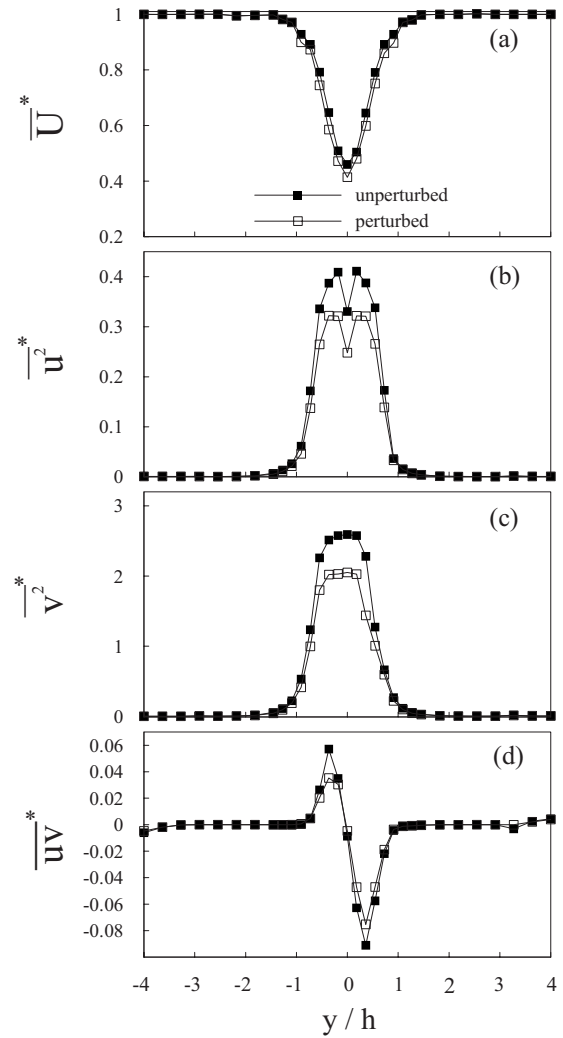
nitude) appears at $f_s'^*$, as the hotwire is located above the leading edge of the test model, i.e., $x/h=-4$ and $y/h=0.75$ [Fig. 10(a)]. Toward the trailing edge, the magnitude of E at $f_s'^*$ continually increases, though still rather small until the hotwire reaches the model trailing edge at $x/h=0$ and $y/h=0.75$ [Figs. 10(b)–10(e)]. The peak value of E at $f_s'^*$ undergoes drastic changes behind the trailing edge of the test model at $x/h=1$, jumping from 0.011 to 0.11 [Fig. 10(f)], where the peaks at the second and third harmonics of $f_s'^*$, i.e., $f_s''^*$ and $f_s'''^*$, are also evident. The measured E at $f_s'^*$ progressively decreases with the increasing x/h but remains much larger than those at $x/h \leq 0$ [Figs. 10(g)–10(j)]. The modification in unperturbed E at $f_s'^*$ can be attributed to the evolution of vortex shedding from the test model. These observations are, in fact, consistent with numerical findings reported by Hourigan et al.[51] and Mills et al.,[52] who observed that flow over an elongated bluff body separated from the plate leading edge and formed vortices. The vortices then reattached on the plate surface and continually moved along it until reaching the plate trailing edge, where they were shed into the wake. On the other hand, as a leading edge vortex approached the trailing edge, the redeveloped thin boundary
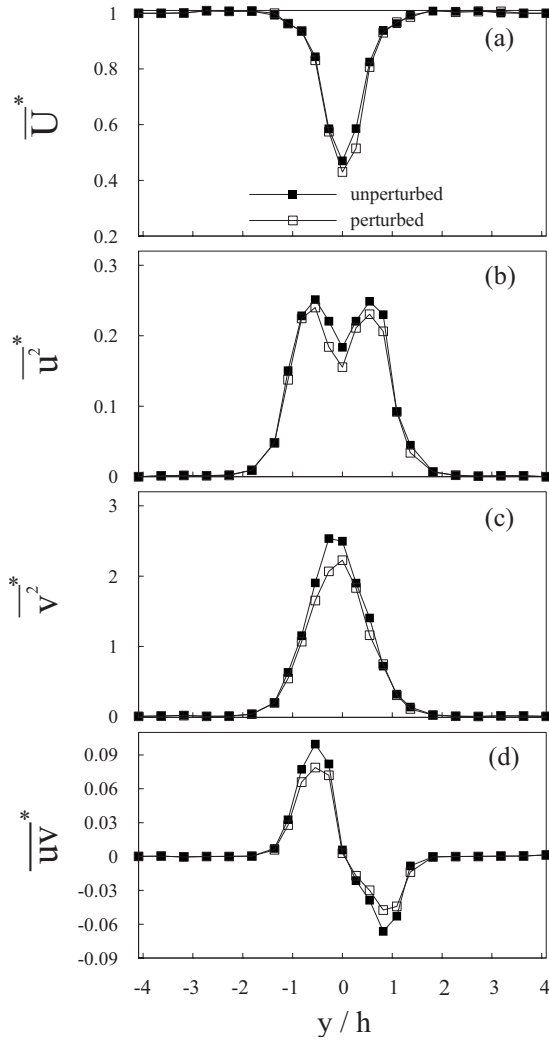
FIG. 9. Cross-flow distribution of mean streamwise flow velocity and Reynolds stresses at $x/h=5$: (a) $\bar{U}^*$, (b) $\overline{u^2}^*$, (c) $\overline{v^2}^*$, (d) $\overline{uv}^*$. Re=6200.
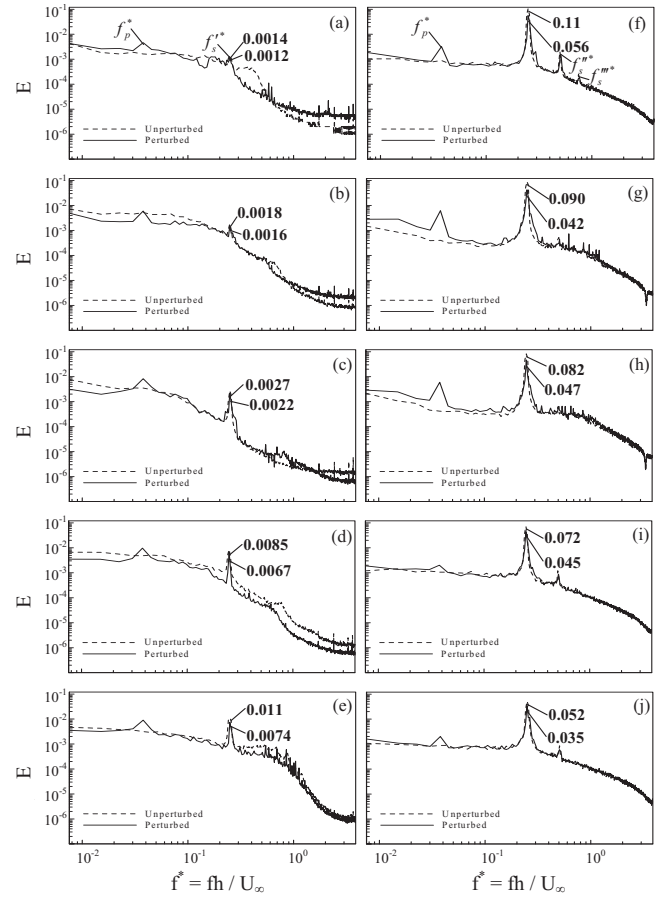

FIG. 10. The fluctuating velocity spectrum E with and without perturbation at different streamwise locations ($y/h=0.75$): (a) $x/h=-4$; (b) $x/h=-3$; (c) $x/h=-2$; (d) $x/h=-1$; (e) $x/h=0$; (f) $x/h=1$; (g) $x/h=2$; (h) $x/h=3$; (i) $x/h=5$; (j) $x/h=7$. Re=6200.

layer in front of it would also separate at the plate trailing edge and rolled up to form a trailing-edge vortex of like sign. The vortices from the leading and trailing edges interact and their interaction occurs alternately on each side of the plate at the upper and lower trailing-edge corners, resulting in a pair of regular vortex streets in the wake. In the present case, the frequency of vortex shedding from the leading/trailing edge is locked-in with f_a'.[53] In addition, the strength of the trailing-edge vortex was much higher than that of the leading edge vortex.[53] This could explain the small peaks in E at $f_s'^*$ over the plate surface and the jump in E at $f_s'^*$ in the wake of the model. Once the perturbation was applied, the perturbation disturbed the redeveloped boundary layer on the plate from which the trailing-edge vortices formed, resulting in a significant reduction in the energy of vortices, especially in the wake of the model (Fig. 10). This statement can be further substantiated by using a more accurate method to quantify the variation in $E_{\Delta f}$ associated with $f_s'^*$ by integrating E over a -3 dB bandwidth about $f_s'^*$ in Fig. 10. The percentage (δ) of energy reduction under control, compared with the uncontrolled case, at different locations are calculated and shown in Fig. 11. It can be seen that the reduction in $E_{\Delta f}$ is most

pronounced at the trailing edge near the model; for example, δ are about 67%, 57%, and 51%, corresponding to $x/h=1$, 2, and 3, respectively. The impaired vortices near the model may be possibly responsible for the considerable decrease in the SPL at f_a', consistent with the results in Fig. 5.
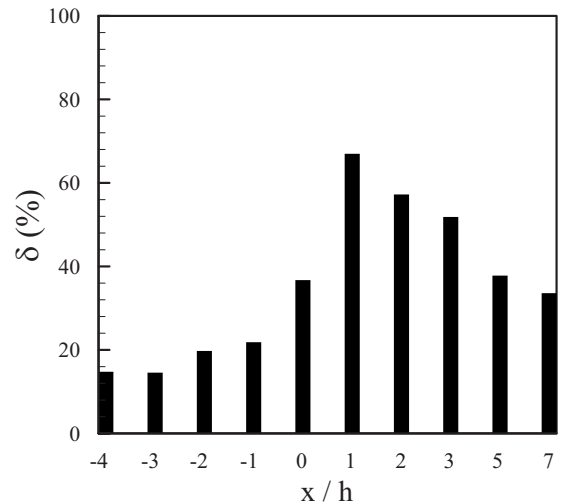

FIG. 11. Comparison in the energy reduction percentage (δ) of the fluctuating flow velocity at different streamwise locations ($y/h=0.75$). Re=6200.
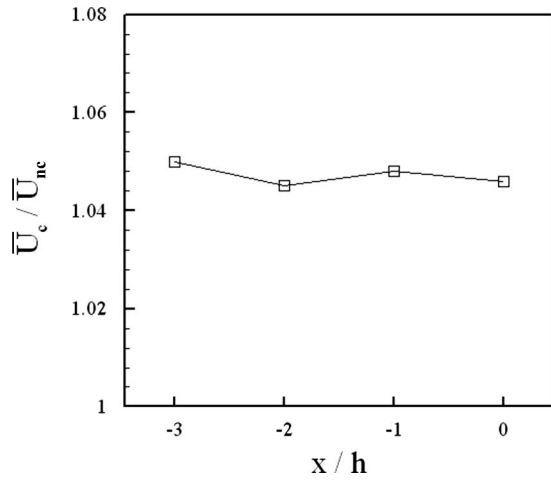
FIG. 12. The streamwise variation of the mean flow velocity under control ($y/h=0.75$). Re=6200.

From the results in Figs. 10 and 11, one may surmise that the weakened vortex street results from the impaired strength of the dominant trailing-edge vortex. To confirm this, the streamwise mean flow velocity above the surface of the model was measured under control ($y/h=0.75$), as indicated in Fig. 12. The measured flow velocity $\bar{U}_c$ exceeds the unperturbed velocity $\bar{U}_{nc}$ by about 5% at $x/h=-3$ to 0. The typical time history of the streamwise total flow velocity signal U, measured by the hotwire placed at $x/h=-3$ and $y/h=0.75$, highlights an increase in $\bar{U}_c$ once the perturbation is introduced (Fig. 13). The perturbation displacement ($Y_{prms}=0.64$ mm) will pump energy into the boundary layer over the plate and lead to transition to turbulence and subsequently early reattachment of the leading edge vortices. This transition may entrain high-speed free-stream fluid to the flow near the plate and increase $\bar{U}_c$. Furthermore, the enhanced $\bar{U}_c$ may accelerate the advection of the leading edge vortex along the model surface, as confirmed by the perturbation effect on the phase shift $\phi_{u_1 u_2}$ (Fig. 14) between two streamwise flow velocities, u_1 and u_2, simultaneously measured using two single hotwires above the model lead-
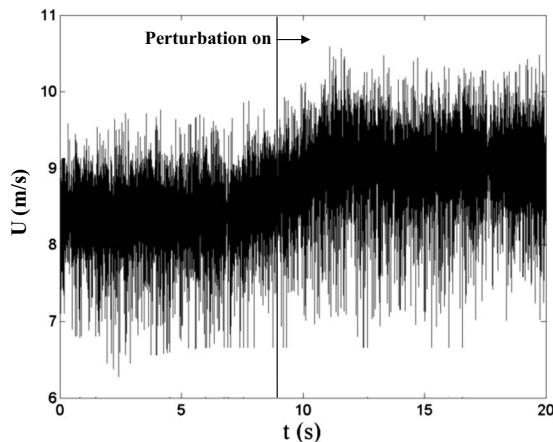

FIG. 13. Typical transition of the total streamwise flow velocity signal U when the perturbation was switched off and on. The hotwire was located at $x/h=-3$ and $y/h=0.75$. Re=6200.
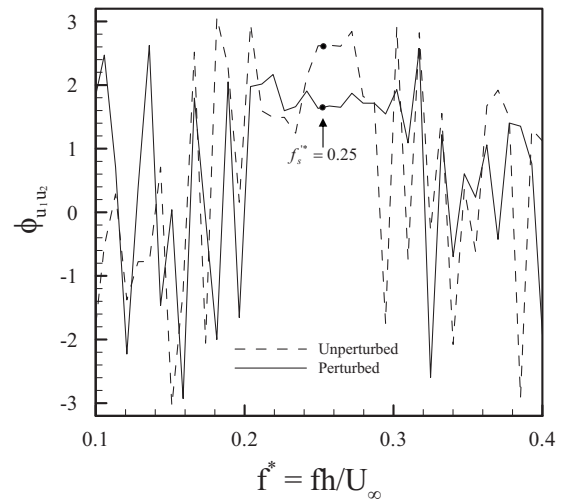

FIG. 14. Spectral phase $\phi_{u_1 u_2}$ between the fluctuating flow velocity (u_1) at $x/h=0$ and $y/h=0.75$ and the fluctuating flow velocity (u_2) at $x/h=-4$ and $y/h=0.75$. Re=6200.

ing edge ($x/h=-4$, $y/h=0.75$) and trailing edge ($x/h=0$, $y/h=0.75$), respectively. Here, $\phi_{u_1 u_2}$ is defined by $\phi_{u_1 u_2}[\equiv \tan^{-1}(Q_{u_1 u_2}/Co_{u_1 u_2})]$, where $Co_{u_1 u_2}$ and $Q_{u_1 u_2}$ are the cospectrum and quadrature spectrum of u_1 and u_2, respectively. The cross-spectrum was computed from the Fourier transform of the correlation $\overline{u_1(t+\tau)u_2(t)}$.[36] Obviously, $\phi_{u_1 u_2}$ at $f_s'^*$ decreases from 2.6 to 1.7 after perturbation. The comparison in $\phi_{u_1 u_2}$ was conducted within 1 cycle of leading edge vortex shedding since w/h was designed such that only one vortex separated from the leading edge of the plate is developed along the plate at any instant.[43] The decreased $\phi_{u_1 u_2}$ implies less time for a vortex to travel from the leading edge to the trailing edge under control. In a test carried out in a water tunnel, Mills et al.[52] introduced a transverse disturbance through the oscillation of the top and bottom walls of the working section to disturb the flow field around a rectangular plate with $w/h=6-10$. Before control, they found that the undisturbed leading edge vortices always passed the plate trailing edge at the same time in one cycle as the leading edge vortex shedding regardless of the w/h value. They further observed that, for steady flow, as the leading edge vortices on one side of the plate passed the corresponding trailing-edge corner, the reattached boundary layer adjacent to the other trailing-edge corner began to roll up, forming trailing-edge vortices, which alternately occurred on both sides of the plate. Based on the observations, they successfully impaired trailing-edge vortices by controlling the disturbance phase within a full disturbance cycle as the leading edge vortices reached the trailing-edge corner. By doing so, the disturbed leading edge vortices at one trailing-edge corner could move downward or upward to interfere with the initial rollup motion of the redeveloped boundary layer from another trailing-edge corner, thus greatly reducing the vortex strength of trailing-edge vortices. Similarly, the present accelerated leading edge vortices on the upper side of the plate may interact with the redeveloped boundary layer separated from the lower trailing-edge corner. Without perturbation, the interaction/disturbance will not occur because the upper

Zhang et al.: Control of acoustic cavity resonance   43

leading edge vortices and lower trailing-edge vortices cannot simultaneously appear near their corresponding trailing-edges. This disturbance of upper leading edge vortices effectively perturbs the rollup of lower trailing-edge vortices by collision, leading to the impaired strength of lower trailing-edge vortices.

As seen in Figs. 8 and 9, the perturbation on the upper side of the model has the equal effect on either side of the wake centerline. This has been observed in other cases[54] and is attributed to the steady formation of vortex streets. In fact, vortex shedding is a result of initial wake instability.[55] In order to form a stable vortex street, it is essential for the two oppositely signed vortices separating from the cylinder to have approximately the same strength through interactions.[56] Therefore, vortex shedding from both sides of the plate appears equally affected.

From a different perspective, the weakened wake behind the model was shown to result in a modification in flow-acoustic correlation. As a matter of fact, the spectral coherence between the fluctuating flow velocity (u) and the fluctuating acoustic pressure (p) showed that the strong correlation between vortex shedding from the model and the first acoustic mode of the cavities receded once the perturbation is introduced.

Based on the above analyses, an interpretation for the impaired vortex-induced acoustic resonance mechanism is now proposed. The vortex-induced acoustic resonance originates from the strong interaction between the coupled vortices shed from both leading and trailing-edges of the bluff body and the first acoustic mode of the cavities. The trailing-edge vortex overwhelms the leading edge vortex in terms of the vortex strength. The asynchronous controlled surface perturbation accelerates the advection of the reattached leading edge vortices along the model surface and thus disturbs the formation of the trailing-edge vortices, leading to a significant reduction in the vortex strength in the wake of the model. The whole process results in an effective impairment in the flow-acoustic interaction and subsequently the vortex-induced acoustic resonance.

VI. CONCLUSIONS

Control of vortex-induced acoustic resonance has been experimentally investigated using a perturbation technique. The investigation leads to following conclusions.

(1) Vortex-induced acoustic resonance may be effectively controlled using an imbedded piezo-electric actuator along with an asynchronous control system; the SPL at the first acoustic resonance was reduced by 8.2 dB.

(2) Analyses of the measured data suggest that the effective control lies in the modification of the vortex strength in the wake of the bluff body. The vortex-induced acoustic resonance results from strong interactions between vortices originated from both leading and trailing-edges of the plate and the acoustic mode of the downstream axisymmetric cavities. The convection of the vortex originated from the leading edge along the plate surface was accelerated by the controllable surface perturbation. This subsequently changes the initial conditions in the forma-

tion of the trailing-edge vortex and further enables a vigorous interaction between the two types of vortices, thus weakening remarkably the vortex strength in the wake of the plate and hence the flow-acoustic interaction.

[1] R. D. Blevins, "The effect of sound and vortex shedding from cylinders," J. Fluid Mech. **161**, 217–237 (1985).

[2] D. Rockwell and E. Naudascher, "Review—Self-sustaining oscillations of flow past cavities," ASME J. Fluids Eng. **100**, 152–165 (1978).

[3] M. S. Howe, *Theory of Vortex Sound* (Cambridge University Press, Cambridge, 2003).

[4] A. Oengören and S. Ziada, "Vorticity shedding and acoustic resonance in an in-line tube bundle, Part II: Acoustic resonance," J. Fluids Struct. **6**, 293–309 (1992).

[5] P. M. Radavich, A. Selamet, and J. M. Novak, "A computational approach for flow-acoustic coupling in closed side branches," J. Acoust. Soc. Am. **109**, 1343–1353 (2001).

[6] K. S. Peat, J. G. Ih, and S. H. Lee, "The acoustic impedance of a circular orifice in grazing flow: Comparison with theory," J. Acoust. Soc. Am. **114**, 3076–3086 (2003).

[7] R. D. Blevins and M. M. Bressler, "Experiments on acoustic resonance in heat exchanger tube bundles," J. Sound Vib. **164**, 503–533 (1993).

[8] R. Parker and D. C. Pryce, "Wake excited resonances in an annular cascade: An experimental investigation," J. Sound Vib. **37**, 247–261 (1974).

[9] S. Ziada, A. Oengören, and A. Vogel, "Acoustic resonance in the inlet scroll of a turbo-compressor," J. Fluids Struct. **16**, 361–373 (2002).

[10] A. Mohany and S. Ziada, "Flow-excited acoustic resonance of two tandem cylinders in cross-flow," J. Fluids Struct. **21**, 103–119 (2005).

[11] L. Cattafesta, D. Williams, C. Rowley, and F. Alvi, "Review of active control of flow-induced cavity resonance," AIAA Paper No. 2003-3567 (2003).

[12] S. A. T. Stoneman, K. Hourigan, A. N. Stokes, and M. C. Welsh, "Resonant sound caused by flow past two plates in tandem in a duct," J. Fluid Mech. **192**, 455–484 (1988).

[13] B. A. W. Simth and B. V. Luloff, "The effect of seat geometry on gate valve noise," ASME J. Pressure Vessel Technol. **122**, 401–407 (2000).

[14] H. H. Heller and D. B. Bliss, "The physical mechanism flow-induced pressure fluctuations in cavities and concepts for the suppression," AIAA Paper No. 75-491 (1975).

[15] S. F. McGrath and D. J. Olinger, "Control of pressure oscillations in deep cavities excited by grazing flow," J. Aircr. **33**, 29–36 (1996).

[16] L. N. Cattafesta III, S. Garg, M. Choudhari, and F. Li, "Active control of flow-induced cavity resonance," AIAA Paper No. 97-1804 (1997).

[17] R. L. Sarno and M. E. Franke, "Suppression of flow-induced pressure oscillations in cavities," J. Aircr. **31**, 90–96 (1994).

[18] X. Y. Huang and D. S. Weaver, "On the active control of shear layer oscillations across a cavity in the presence of pipeline acoustic resonance," J. Fluids Struct. **5**, 207–219 (1991).

[19] S. Ziada, H. Ng, and C. E. Blake, "Flow excited resonance of a confined shallow cavity in low Mach number flow and its control," J. Fluids Struct. **18**, 79–92 (2003).

[20] L. N. Cattafesta III, S. Garg, and D. Shukla, "The development of piezo-electric actuators for active flow control," AIAA J. **39**, 1562–1568 (2001).

[21] L. N. Cattafesta III, J. Mathew, and A. Kurdila, "Modeling and design of piezoelectric actuators for fluid flow control," Trans. Jpn. Soc. Aeronaut. Space Sci. **109**, 1088–1095 (2001).

[22] H. Kook, L. Mongeau, and M. A. Franchek, "Active control of pressure fluctuations due to flow over Helmholtz resonators," J. Sound Vib. **255**, 61–76 (2002).

[23] N. B. Roozen, M. Bockholts, V. E. Pascal, and A. Hirschberg, "Vortex sound in bass-reflex ports of loudspeakers. Part I. Observation of response to harmonic excitation and remedial measures," J. Acoust. Soc. Am. **104**, 1914–1918 (1998).

[24] M. M. Zdravkovich, "Review and classification of various aerodynamic

and hydrodynamic means for suppressing vortex shedding," J. Wind. Eng. Ind. Aerodyn. **7**, 145–189 (1981).

[25]J. Every, R. King, and D. S. Weaver, "Vortex-excited vibrations of cylinders and cables and their suppression," Ocean Eng. **9**, 135–157 (1982).

[26]F. Wilson and J. C. Tinsley, "Vortex load reduction: experiments in optimal helical strake geometry for rigid cylinders," ASME J. Energy Resour. Technol. **111**, 72–76 (1989).

[27]F. B. Hsiao and J. Y. Shyu, "Influence of internal acoustic excitation upon flow passing a circular cylinder," J. Fluids Struct. **5**, 427–442 (1991).

[28]D. R. Williams, H. Mansy, and C. Amato, "The response and symmetry properties of a cylinder wake subjected to localized surface excitation," J. Fluid Mech. **234**, 71–96 (1992).

[29]H. M. Warui and N. Fujisawa, "Feedback control of vortex shedding from a circular cylinder by cross-flow cylinder oscillations," Exp. Fluids **21**, 49–56 (1996).

[30]P. T. Tokumaru and P. E. Dimotakis, "Rotary oscillation control of a cylinder wake," J. Fluid Mech. **224**, 77–90 (1991).

[31]J. R. Filler, P. L. Marston, and W. C. Mih, "Response of the shear layers separating from the circular cylinder to small amplitude rotational oscillations," J. Fluid Mech. **231**, 481–499 (1991).

[32]J. E. Ffowcs Williams and B. C. Zhao, "The active control of vortex shedding," J. Fluids Struct. **3**, 115–122 (1989).

[33]K. Roussopoulos, "Feedback control of vortex shedding at low Reynolds numbers," J. Fluid Mech. **248**, 267–296 (1993).

[34]X. Y. Huang, "Feedback control of vortex shedding from a circular cylinder," Exp. Fluids **20**, 218–224 (1996).

[35]L. Cheng, Y. Zhou, and M. M. Zhang, "Perturbed interaction between vortex shedding and induced vibration," J. Fluid Mech. **17**, 887–901 (2003).

[36]M. M. Zhang, L. Cheng, and Y. Zhou, "Closed-loop-controlled vortex shedding from a flexibly supported square cylinder under different schemes," Phys. Fluids **16**, 1439–1448 (2004).

[37]M. M. Zhang, L. Cheng, and Y. Zhou, "Closed-loop-controlled vortex shedding from a flexibly supported square cylinder under different schemes," Eur. J. Mech. B/Fluids **23**, 189–197 (2004).

[38]M. M. Zhang, L. Cheng, and Y. Zhou, "Control of vortex-induced non-resonance vibration using piezo-ceramic actuators embedded in a structure," Smart Mater. Struct. **14**, 1217–1226 (2005).

[39]L. Cheng, Y. Zhou, and M. M. Zhang, "Controlled vortex-induced vibration on a fix-supported flexible cylinder in crossflow," J. Sound Vib. **292**, 279–299 (2006).

[40]M. M. Zhang, L. Cheng, and Y. Zhou, "Closed-loop controlled vortex-airfoil interactions," Phys. Fluids **18**, 046102 (2006).

[41]M. M. Zhang, L. Cheng, and Y. Zhou, "Control of post-stall airfoil aerodynamics based on surface perturbation," AIAA J. **46**, 2510–2519 (2008).

[42]Y. S. Choy and L. Huang, "Effect of flow on the drumlike silencer," J. Acoust. Soc. Am. **118**, 3307–3085 (2005).

[43]R. Parker and M. C. Welsh, "Effects of sound on flow separation from blunt flat plates," Int. J. Heat Fluid Flow **4**, 113–127 (1983).

[44]M. C. Welsh, A. N. Stokes, and R. Parker, "Flow-resonant sound interaction in a duct containing a plate, Part I: Semi-circular leading edge," J. Sound Vib. **95**, 305–323 (1984).

[45]S. Ziada and S. Shine, "Strouhal numbers of flow-excited acoustic resonance of closed side branches," J. Fluids Struct. **13**, 127–142 (1999).

[46]J. P. Marouzé and L. Cheng, "A feasibility study of active vibration isolation using THUNDER actuators," Smart Mater. Struct. **11**, 854–862 (2002).

[47]O. Durgun and K. Kafali, "Blockage correction," Ocean Eng. **18**, 269–282 (1991).

[48]J. C. Bruggeman, A. Hirschberg, M. E. H. Van Dongen, A. P. J. Wijnands, and J. Gorter, "Self-sustained aero-acoustic pulsations in gas transport systems: Experimental study of the influence of closed side branches," J. Sound Vib. **150**, 371–393 (1991).

[49]P. M. Morse, *Vibration and Sound* (American Institute of Physics for the Acoustical Society of America, New York, 1981).

[50]S. A. Wise, "Displacement properties of RAINBOW and THUNDER piezoelectric actuators," Adv. Weld. Sci. Technol., Proc. Int. Conf. Trends Weld. Res. **69**, 33–38 (1998).

[51]H. Hourigan, M. C. Thompson, and B. T. Tan, "Self-sustained oscillations in flows around long blunt plates," J. Fluids Struct. **15**, 387–398 (2001).

[52]R. Mills, J. Sheridan, and K. Hourigan, "Particle image velocimetry and visualization of natural and forced flow around rectangular cylinders," J. Fluid Mech. **478**, 299–323 (2003).

[53]A. N. Stokes and M. C. Welsh, "Flow-resonant sound interaction in a duct containing a plate, II: Square leading edge," J. Sound Vib. **104**, 55–73 (1986).

[54]C. Welsh, K. Hourigan, L. W. Welch, R. J. Downie, M. C. Thompson, and A. N. Stokes, "Acoustics and experimental methods: The influence of sound on flow and heat transfer," Exp. Therm. Fluid Sci. **3**, 138–152 (1990).

[55]M. Provansal, C. Mathis, and L. Boyer, "Benard–von Kámán instability: Transient and forced regimes," J. Fluid Mech. **182**, 1–22 (1987).

[56]H. Sakamoto, K. Tan, and H. Haniu, "An optimum suppression of fluid forces by controlling a shear layer separated from a square prism," J. Fluids Eng. **113**, 183–189 (1991).